coatings

MDPI

Article

SERS Activity of Silver Nanosphere, Triangular Nanoplates, Hexagonal Nanoplates and Quasi-Spherical Nanoparticles: Effect of Shape and Morphology

Marco Zannotti *, Andrea Rossi and Rita Giovannetti *

School of Science and Technology, Chemistry Division, University of Camerino, 62032 Camerino, Italy; andrea.rossi@unicam.it

* Correspondence: marco.zannotti@unicam.it (M.Z.); rita.giovannetti@unicam.it (R.G.)

Received: 18 February 2020; Accepted: 18 March 2020; Published: 20 March 2020

Abstract: In this work, we prepared different morphologies of silver nanoparticles: nanosphere, triangular nanoplates, hexagonal nanoplates, and quasi-spherical shapes, through one-step synthesis. Hydrogen peroxide was used as the oxidizing agent during the reduction of silver nitrate by sodium borohydride, in the presence of tri-sodium citrate and poly-vinyl-pyrrolidone. The obtained silver nanoparticles were fully characterized by UV-Vis spectroscopy, Dynamic Light Scattering and Scanning Electron Microscopy, and successfully used as Surface Enhanced Raman Scattering (SERS) substrates. The effect of shape and morphology on the Raman scattering enhancement was evaluated by using methylene blue as target molecules. The Raman measurements demonstrated that the prepared substrates are reliable and sensitive with analytical enhancement factors, estimated to be around 10^5 with a concentration of methylene blue 1 μM. When triangular and hexagonal nanoplates were tested with different concentrations of analyte, they demonstrated a good linearity in Raman intensity with a good detection of methylene blue 0.1 μM.

Keywords: silver nanoplates; SERS; anisotropic structures; methylene blue; H_2O_2

1. Introduction

Raman spectroscopy is a fast and efficient technique for materials characterization and molecules identification; this technique gives information about vibrational and rotational molecular modes by the detection of inelastic scattering, produced by the interaction of monochromatic light as a laser and the electrons of sample molecules.

Nevertheless, the Raman scattering is not very high, and this limitation prevents its use for the detection of low analyte concentrations [1]. For this reason, Surface Enhanced Raman Scattering (SERS) is a powerful vibrational spectroscopic technique that can extend the sensitivity of conventional Raman spectroscopy to the single molecule level [2–4]. The power of SERS can be exploited for its versatility and feasibility in a wide variety of fields including polymers, materials science, biochemistry and bio-sensing, catalyst, electrochemistry, pesticides, and food additives [5–9]. SERS technique increases drastically the Raman signals of an analyte molecule by the presence of roughened metal noble-metals (Ag and Au) near or in proximity of the analyzed samples [10,11].

Two mechanisms are responsible for the signal improvement: Electromagnetic (EM) and Chemical Enhancement (CE). The first one is related to the amplification of electromagnetic fields, generated by the excitation of the Localized Surface Plasmon Resonance (LSPR) of the noble nanoparticles; this phenomenon is responsible for the great enhancement of Raman scattering during SERS and can reach Enhancement Factors (EF) around 10^8 [12,13]. The Chemical Enhancement results from

the electronic resonance charge transfer between metal nanoparticles and the molecule; in this case, the SERS enhancement is considerably lower with respect to the EM, with EF around 10-100 [12].

Noble metal nanoparticles show strong LSPR in the Visible and near-IR region, rendering them suitable for many applications [14], and in particular as SERS substrates. The LSPR is correlated to the size and shape of the noble metal nanoparticles and these two factors play an important role in the SERS enhancement [15].

The Raman scattering enhancement is attributed to the generation of local electromagnetic field "hotspots", due to the surface roughness of the materials and the shape of nanoparticles, coupled with LSPR excitation [16]. In fact, the high curvature surface, irregular surface and sharper edges exhibit a great enhancement of the Raman scattering by generating a local high electromagnetic field enhancement, demonstrating the importance of metal nanoparticles synthesis [11,12,16,17]. In this sense, silver nanostars, nanocubes, prisms, or nanoparticles with defects have demonstrated high sensitivity and high enhancement of the Raman signals showing higher potential, with respect to spherical nanoparticles with the same dimensions [12,18–23].

In this work, we studied the different morphologies of silver nanoparticles (AgNPs): nanosphere, triangular nanoplates, hexagonal nanoplates, and quasi-spherical shapes, prepared by one-step synthesis by using hydrogen peroxide as the etchant and sodium borohydride as the reducing agent.

The AgNPs were fully characterized by UV-Vis spectroscopy, Dynamic Light Scattering (DLS) and Scanning Electron Microscopy (SEM). The SERS substrates were prepared by using the AgNPs mentioned before, and the effect of shape and morphology on the Raman scattering enhancement was evaluated by using Methylene Blue (MB) as target molecules.

2. Materials and Methods

Silver Nitrate ($AgNO_3$), Sodium Borohydride ($NaBH_4$), Tri-Sodium Citrate (TSC), Poly-Vinyl Pyrrolidone (PVP), Hydrogen Peroxide (H_2O_2) and Methylene Blue were purchased from Sigma-Aldrich and used without further purification. All solutions and dilutions were prepared using deionized water.

2.1. Synthesis of Silver Nanoparticles

Silver nanoparticles were prepared by a chemical reduction method in aqueous solution: with a total volume of 10 mL, $AgNO_3$ (0.16 mM), PVP (0.16 mM), TSC (2.7 mM), different amounts of H_2O_2 (0, 39, 78 and 142 mM) and $NaBH_4$ (0.98 mM) were mixed. After stirring for 30 min, stable solutions of AgNPs were obtained. Before their use, the AgNPs solutions were centrifuged at 22,000 rcf in order to eliminate the excess of TSC and PVP. The samples were named with a number that reflects the concentration (mM) of H_2O_2 used during the synthesis. The AgNPs solutions were prepared in three replicates and validated by UV-Vis spectroscopy.

2.2. Characterization of AgNPs

The AgNPs solutions were characterized by UV-Vis Spectroscopy and Dynamic Light Scattering using a Hewlett–Packard 845D Diode Array spectrophotometer and a Malvern Zetasizer nanoS, equipped with a back-scattered light detector operating at 173°, respectively.

The morphology of the AgNPs was evaluated by SEM analysis. The AgNPs were placed on aluminum stubs using self-adhesive carbon conductive tabs, dried in a vacuum oven (Vismara, 65) at 40°C, and analyzed with Field Emission Scanning Electron Microscopy (FE-SEM, Sigma Family, Zeiss) operated at 7 kV, equipped with Energy Dispersive X-ray spectroscopy (EDX, Quantax, EDS, Bruker).

2.3. SERS Substrate Preparation

In order to prepare SERS substrates, microscope glass slides (Pearl, 25.4 × 76.2 mm^2, 1.2 mm thick) were previously washed in order to eliminate contaminants and successively, a bottom layer of specific AgNPs was prepared by multiple additions of 2 µL (immediately dried in the oven at 40 °C) with a total silver amount equal to 0.0035 mg. Successively, an upper layer of MB was added to the obtained

SERS substrates by multiple additions of MB 2 µL (immediately dried in the oven at 40 °C), in order to maintain a ratio of vAgNPs/vMB at 3:1.

2.4. SERS—Raman Setup

Raman analysis was performed by a micro-Raman spectrometer (iHR320, Horiba), using a red laser at 632.82 nm wavelength. All the measurements were performed at room temperature at a laser power of 30 mW, and the objective outlet was 50X (Olympus, LMPLFLN50 X, NA = 0.5; wd = 10.6 mm). Before the measurements, the Raman spectrometer was always calibrated with a silicon calibration standard, by monitoring the Raman peak at 520.7 cm^{-1}.

A Raman spectrum of MB 1×10^{-2} M, without AgNPs as the SERS activator, was recorded with 10 sec of acquisition time and 3 accumulations. SERS spectra of MB 1×10^{-6} M and 1×10^{-7} M were recorded with 10 sec of acquisition time and 3 accumulations.

3. Results and Discussion

3.1. Nanoparticles Characterization

AgNPs with different shapes and nanostructures were synthesized exploiting the erosion effect of H_2O_2, that act as the oxidizing agent during the reduction of $AgNO_3$ by $NaBH_4$, in the presence of TSC and PVP, as the capping and dispersing agent, respectively [24]. The synthesized AgNPs showed distinct colors that reflect different UV-Vis spectra, which are reported in Figure 1. The AgNPs-0 showed a yellow color of the solution and exhibits the typical spectrum of spherical nanoparticles with a LSPR band at 413 nm [25].

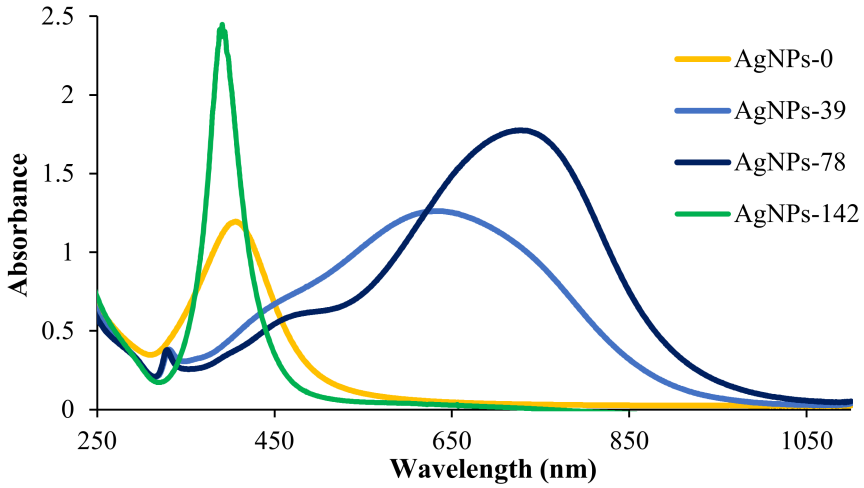

Figure 1. UV-Vis spectra of AgNPs-0, AgNPs-39, AgNPs-78 and AgNPs-142.

The AgNPs-39 shows three different bands at 330, 440 and 640 nm, assigned to the out-of-plane quadrupole, in-plane quadrupole and in-plane dipole plasmon resonance, respectively, typical of silver nanoplates [26]. With the addition of higher amounts of H_2O_2, the AgNPs-78 exhibits always three bands, the first one remains unchanged at 330 nm, while the other two bands resulted in red-shift to longer wavelengths at 470 and 726 nm, confirming also in this case the presence of silver nanoplates. The observed shift of the AgNPs-78 sample with respect to AgNPs-39 probably indicates a different size or morphology of the nanoplates. AgNPs-39 and AgNPs-78 showed different shades of blue colors, as reported in the pictures inserted in Figure 2d,g.

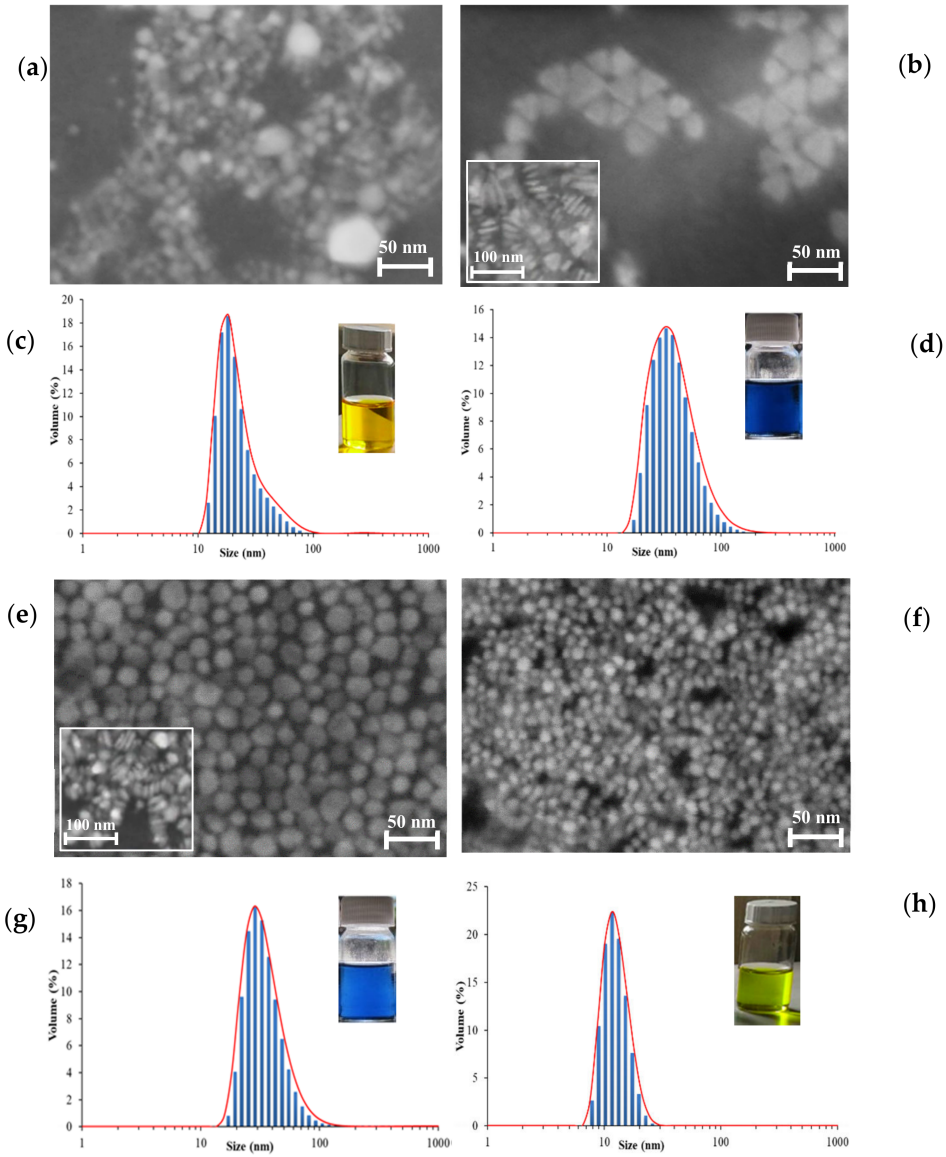

Figure 2. SEM images and DLS spectra of (**a**,**c**) AgNPs-0; (**b**,**d**) AgNPs-39; (**e**,**g**) AgNPs-78; and (**f**,**h**) AgNPs-142.

With addition of H_2O_2 142 mM, the colloidal solution showed a yellow-green color with a blue-shifted LSPR band at 393 nm (Figure 1), indicating a spherical shape of the nanoparticles, with a more uniform distribution due to the narrowed band.

The anisotropic structures and the different shapes of AgNPs were confirmed by Scanning Electron Microscopy and the obtained SEM images are reported in Figure 2, where the poor resolution is due to the presence of a small amount of PVP, which still remained, even after the centrifugation.

In Figure 2a are the visualized morphologies of AgNPs-0 showing mixed spherical shapes with a diameter of around 15 nm, with the presence of larger nanoparticles at around 40 nm. The AgNPs-39 sample (Figure 2b) shows high anisotropic structures, like triangular nanoplates with sides of 35–40 nm and a thickness of about 5 nm. In addition, hexagonal nanoplates displaying sides and a thickness of 25–30 and 3–4 nm, respectively, are obtained with AgNPs-78. The AgNPs-142 (Figure 2d) shows 3D-structure as quasi-spherical shapes with a diameter of around 10 nm, with no well-defined profile, interpretable as morphological defects. The DLS analysis was consistent with the results obtained by SEM and are reported in Figure 2c,d,g,h. The polydispersity index (PdI), reported in Table 1, shows that the samples were monodispersed, and the higher PdI value of AgNPs-0 was due probably to the

presence of several aggregates inside the sample. The results obtained by SEM images describe that, by using different amounts of H_2O_2 as the etchant during the reduction process, nanoparticles with different sizes and shapes can be obtained.

The measured pH of each colloid solution was around neutrality 7.2–7.5.

Both in acidic and basic mediums, the hydrogen peroxide shows high standard redox potentials with respect to Ag (0), as reported in the following reactions [27]:

$$\begin{array}{ll} H_2O_2 + 2H^+ + 2e^- \rightleftarrows 2H_2O & E^0 = +1.7736\ V \\ H_2O_2 + 2e^- \rightleftarrows 2OH^- & E^0 = +0.867\ V \\ Ag + e^- \rightleftarrows Ag & E^0 = +0.7996\ V \end{array}$$

thus, during the formation of the silver nanoparticles, H_2O_2 can act as the oxidizing agent and etches the AgNPs by tuning the shapes and sizes of nanoparticles:

$$\begin{array}{ll} H_2O_2 + 2Ag \rightleftarrows 2Ag^+ + 2H_2O & \Delta E^0 = +0.974\ V \text{ acidic solution} \\ H_2O_2 + 2Ag \rightleftarrows 2Ag^+ + OH^- & \Delta E^0 = +0.07\ V \text{ basic solution} \end{array}$$

In this condition, with a higher amount of H_2O_2, the erosion effect, observed0 in the case of AgNPs-142, was so strong, permitting therefore the formation of quasi-spherical shapes with defects and a lower diameter with respect to AgNPs-0, synthesized in the absence of H_2O_2.

Names, schematic morphology, diameters and PdI index of the obtained AgNPs are summarized in Table 1.

Table 1. Morphology and diameter of synthesized AgNPs.

Sample	Morphology	SEM [a] Diameter (nm)	DLS Diameter (nm)	PdI [b]
AgNPs-0		15	18.2 ± 0.94	0.592
AgNPs-39		35–40	32.2 ± 0.71	0.471
AgNPs-78		25–30	22.3 ± 0.91	0.486
AgNPs-142		10	15.7 ± 0.74	0.478

[a] Size measured by ImageJ software. [b] Polydispersity index measured by Dynamic Light Scattering.

3.2. SERS Analysis

The AgNPs characterized before were used as SERS substrates for the detection of methylene blue as target molecules by using a 632.83 nm laser. The characteristic peaks of MB can be easily detected at a very low concentration (1×10^{-6} M), as reported in the Raman spectra shown in Figure 3. The bands assignment relative to MB are summarized in Table 2.

All the AgNPs substrates show SERS activity (Figure 3) with the greatest increase of Raman signal in the presence of AgNPs-39. The Raman enhancement for MB 1 μM increased in the following order: AgNPs-0, AgNPs-78, AgNPs-142, AgNPs-39 (Table 3). The sequence of the Raman enhancement described by shape order is: mixed spherical nanoparticles, hexagonal, quasi-spherical, triangles, with triangle nanoplates giving the best results as the SERS activator. The characteristic peaks in the SERS spectra of MB 1 μM are consistent with those present in the normal Raman spectrum of MB 0.01 M;

no red or blue shift are observed with the silver substrates, and also, the relative intensity of the Raman shifts remain unchanged.

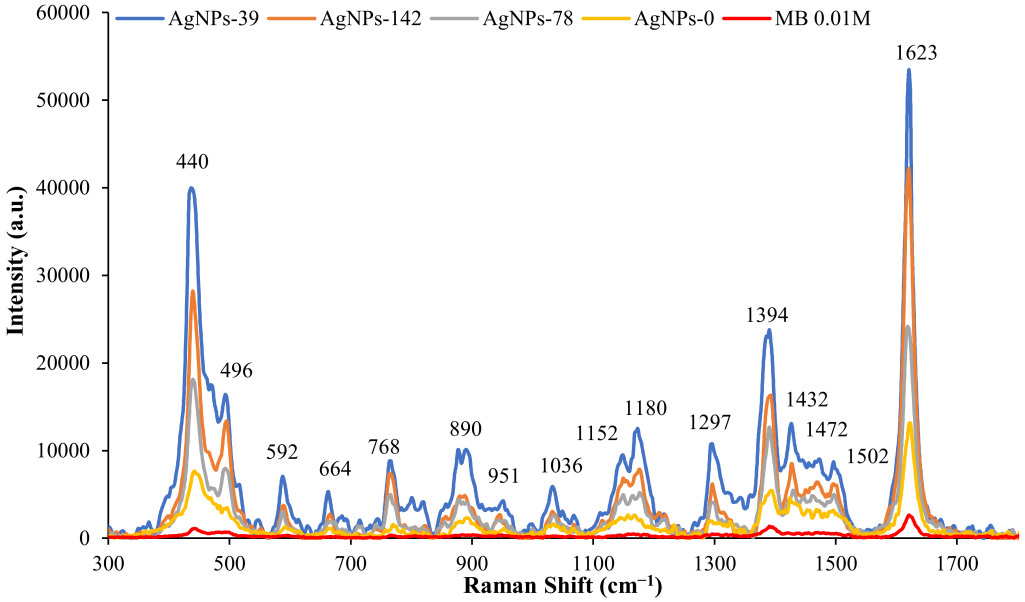

Figure 3. SERS spectra of MB 1 μM with AgNPs-0 (yellow), AgNPs-78 (grey), AgNPs-142 (orange), AgNPs-39 (blue) and the normal Raman spectrum of MB 0.01 M (red).

Table 2. Raman shifts and band assignments for Methylene Blue.

Raman Shifts (cm^{-1})	Band Assignments
440 (s)	Skeletal deformation of C-N-C
496 (m)	Skeletal deformation C-N-C
592 (w)	Skeletal deformation of C-S-C
664 (w)	Out-of-plane bending of C-H
768 (w)	In-plane bending of C-H
890 (w)	In-plane bending of C-H
951(w)	In-plane bending of C-H
1036 (w)	In-plane bending of C-H
1152(w)	In-plane bending of C-H
1180 (w)	Stretching of C-N
1297 (w)	In-plane ring deformation of C-H
1394 (m)	Symmetrical stretching of C-N
1432 (w)	Asymmetrical stretching of C-N
1472 (w)	Asymmetrical stretching of C-N
1502 (w)	Asymmetrical stretching of C-C
1623 (s)	Ring stretching of C-C

Abbreviations: s, strong; m, medium; w, weak peak intensity.

The Analytical Enhancement Factor (AEF) was calculated experimentally by performing the SERS and normal Raman spectra under identical conditions, using the following equation [28]:

$$\mathrm{AEF} = \frac{\mathrm{I_{SERS}}/c_{\mathrm{SERS}}}{\mathrm{I_{RS}}/c_{\mathrm{RS}}}$$

where $\mathrm{I_{SERS}}$ and c_{RS} are the SERS intensity and the concentration of MB (1 μM) used with AgNPs, respectively, while $\mathrm{I_{RS}}$ and c_{RS} are the normal Raman intensity and the concentration of MB (0.01 M) under normal condition, respectively. The AEF results, calculated for the strong vibrations of MB at 1623 and 440 cm^{-1}, for all the prepared SERS substrates, are reported in Table 3, showing that the best

SERS substrate activator was obtained with the AgNPs-39. The AEFs for all the Raman bands of MB (1 μM) are reported in Tables S1–S4.

Table 3. Raman and SERS intensity of MB 1 μM and the calculated AEF at 440 and 1623 cm^{-1}.

Normal Raman MB 0.01 M SERS Substrate (MB 1uM)	I_{1623} **2635.57** I_{1623}	I_{440} **1085.33** **AEF (× 10^5)**	I_{440}	**AEF (× 10^5)**
AgNPs-0	13126	0.50	7654.16	0.71
AgNPs-78	24130.5	0.92	18111.8	1.67
AgNPs-142	40742.7	1.55	28186.4	2.60
AgNPs-39	53480.1	2.03	39952.3	3.68

The high anisotropic structure of triangle nanoplates is a key feature that gives, to the AgNPs-39 substrate, high SERS activity. The curvature and sharp edges of the AgNPs-39, as demonstrated by SEM images, promote the so-called lighting rod effect due to the localization of stronger near-field enhancements at their vertices [29] and are suitable hotspots candidates for high enhancement of Raman signal with the final result of higher AEFs.

In addition, since the excitation source at 632.83 nm is close to the in-plane dipole plasmon of AgNPs-39 (Figure 1), this property can also contribute to the higher AEFs with respect to the other nanoparticles. The second best sample in terms of AEF was AgNPs-142, where the oxidation etching was so strong at reobtaining quasi-spherical nanoparticles, with an LSPR band at 393 nm; in this case, the plasmon resonance band is quite far from the excitation wavelength. Therefore, the high AEFs for AgNPs-142 could be attributed to the great number of "hotspots" on the surface of the nanoparticles associated with a high increase of local electromagnetic field; this is probably due to a large degree of defects and the curvature produced on the nanoparticles surface by the oxidation etching operated by H_2O_2 [11]. AgNPs-78 showed lower AEFs with respect to AgNPs-39 and AgNPs-142; in this case, the anisotropic structures as hexagonal nanoplates give suitable "hotspots" for the enhancement of local electromagnetic field but probably in less number with respect to the other samples. On the other hand, the spherical nanoparticles of AgNPs-0 show the lower enhancement of the Raman signal, which can be due to the absence of suitable "hotspots". In this case, the SERS activity is principally due to the EM enhancement normally shown by noble metallic nanoparticles.

The performances of AgNPs-39 and AgNPs-142 were also tested with different concentrations of MB from 0.1 to 1 μM, and the obtained spectra demonstrated an increase in Raman intensity, as reported in Figure 4a, Figure 5a, where the relative calibration curves for the strongest Raman vibrations at 440 and 1623 cm^{-1} show good correlations (Figure 4b, Figure 5b).

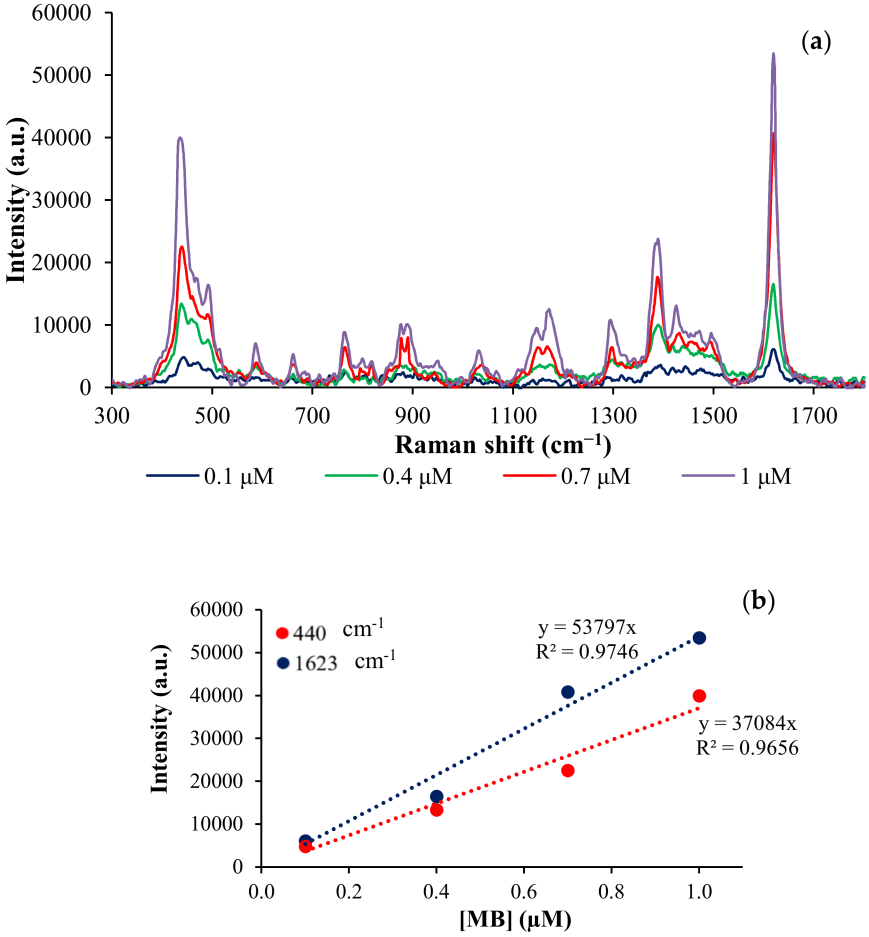

Figure 4. (**a**) SERS spectra of MB with different concentration: 0.1 (blue), 0.4 (green), 0.7 (red) and 1 µM (violet), using AgNPs-39 as SERS substrate, (**b**) calibration curve of SERS intensity at 440 and 1623 cm^{-1}.

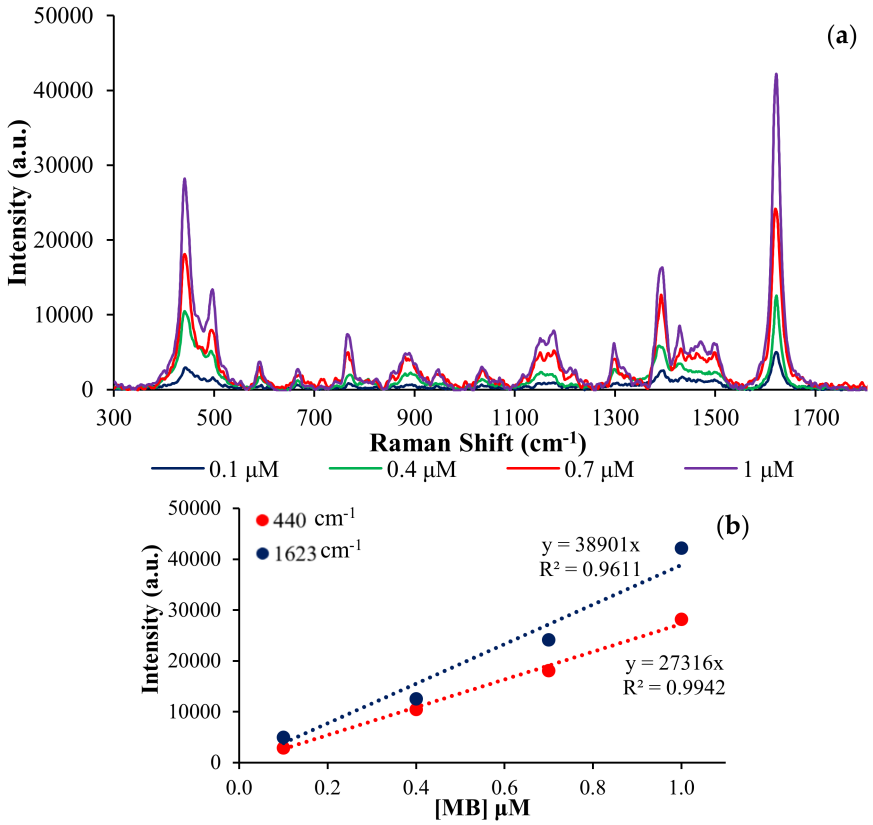

Figure 5. (**a**) SERS spectra of MB with different concentration: 0.1 (blue), 0.4 (green), 0.7 (red) and 1 µM (violet), using AgNPs-142 as SERS substrate, (**b**) calibration curve of SERS intensity at 440 and 1623 cm^{-1}.

4. Conclusions

In summary, by modulation, the erosion effect of H_2O_2, during the reduction of $AgNO_3$ by $NaBH_4$, and in the presence of TSC and PVP, different morphologies of nanoparticles and nanoplates were obtained through an easy one-step synthesis.

The prepared AgNPs were applied in the preparation of substrates for the SERS applications and all of the AgNPs exhibited prominent Raman enhancement at low concentrations of MB as 1 µM. The SERS activity was sensitive to the different AgNPs morphology and, in particular, the Raman enhancement increased in the following order: mixed spherical nanoparticles, hexagonal, quasi-spherical with defects, triangles, with the triangular nanoplates showing the best AEFs.

When triangular and quasi-spherical AgNPs with defects were tested with different concentrations of MB, high correlation with Raman intensity with a good detection of MB 0.1 µM was obtained, demonstrating that this procedure can be effectively used for reliable quantitative SERS analyses.

Supplementary Materials: The following are available online at http://www.mdpi.com/2079-6412/10/3/288/s1, Table S1:Raman and SERS intensity of MB 0.1 µM and the calculated AEFs with AgNPs-39 as SERS substrate; Table S2:Raman and SERS intensity of MB 0.1 µM and the calculated AEFs with AgNPs-142 as SERS substrate; Table S3:Raman and SERS intensity of MB 0.1 µM and the calculated AEFs with AgNPs-78 as SERS substrate; Table S4:Raman and SERS intensity of MB 0.1 µM and the calculated AEFs with AgNPs-0 as SERS substrate.

Author Contributions: R.G. and M.Z. proposed and designed the experiments, A.R. and M.Z. synthesize and characterized the nanoparticles and performed the Raman analysis, A.R. prepared the substrate, M.Z. and R.G. wrote the paper. All the authors participated in discussions of the research. All authors have read and agreed to the published version of the manuscript.

Acknowledgments: The authors are grateful to the School of Science and Technology of University of Camerino for the support and scientific resources like FE-SEM and Raman spectroscopy equipment.

Conflicts of Interest: The authors declare no conflict of interest.

References

1. Okeil, S.; Schneider, J.J. Controlling surface morphology and sensitivity of granular and porous silver films for surface-enhanced Raman scattering, SERS. *Beilstein J. Nanotechnol.* **2018**, *9*, 2813–2831. [CrossRef] [PubMed]
2. Kneipp, K.; Kneipp, H.; Kneipp, J. Surface-Enhanced Raman Scattering in Local Optical Fields of Silver and Gold Fields of Silver and Gold Nanoaggregates—From Single-Molecule Raman Spectroscopy to Ultrasensitive Probing in Live Cells. *Acc. Chem. Res.* **2006**, *39*, 443–450. [CrossRef] [PubMed]
3. Almehmadi, L.M.; Curley, S.M.; Tokranova, N.A.; Tenenbaum, S.A.; Lednev, I.K. Surface Enhanced Raman Spectroscopy for Single Molecule Protein Detection. *Sci. Rep.* **2019**, *9*, 12356–12359. [CrossRef] [PubMed]
4. Khoury, C.G.; Vo-Dinh, T. Gold Nanostars for Surface-Enhanced Raman Scattering: Synthesis, Characterization and Optimization. *J. Phys. Chem. C* **2008**, *112*, 18849–18859. [CrossRef] [PubMed]
5. Sharma, B.; Frontiera, R.R.; Henry, A.-I.; Ringe, E.; Van Duyne, R.P. SERS: Materials, applications, and the future. *Mater. Today* **2012**, *15*, 16–25. [CrossRef]
6. Zhang, W.; Jiang, L.; Piper, J.A.; Wang, Y. SERS Nanotags and Their Applications in Biosensing and Bioimaging. *J. Anal. Test.* **2018**, *2*, 26–44. [CrossRef]
7. Tsai, M.-H.; Lin, Y.-K.; Luo, S.-C. Electrochemical SERS for in Situ Monitoring the Redox States of PEDOT and Its Potential Application in Oxidant Detection. *ACS Appl. Mater. Interfaces* **2018**, *11*, 1402–1410. [CrossRef]
8. Pang, S.; Yang, T.; He, L. Review of surface enhanced Raman spectroscopic (SERS) detection of synthetic chemical pesticides. *TrAC Trends Anal. Chem.* **2016**, *85*, 73–82. [CrossRef]
9. Ai, Y.-J.; Liang, P.; Wu, Y.-X.; Dong, Q.-M.; Li, J.-B.; Bai, Y.; Xu, B.-J.; Yu, Z.; Ni, D. Rapid qualitative and quantitative determination of food colorants by both Raman spectra and Surface-enhanced Raman Scattering (SERS). *Food Chem.* **2018**, *241*, 427–433. [CrossRef]
10. Darienzo, R.E.; Chen, O.; Sullivan, M.; Mironava, T.; Tannenbaum, R. Au nanoparticles for SERS: Temperature-controlled nanoparticle morphologies and their Raman enhancing properties. *Mater. Chem. Phys.* **2020**, *240*, 122143. [CrossRef]
11. Darienzo, R.; Mironava, T.; Tannenbaum, R. Raman Signal Enhancement by Quasi-Fractal Geometries of Au Nanoparticles. *J. Nanosci. Nanotechnol.* **2019**, *19*, 4740–4746. [CrossRef] [PubMed]
12. Dharmalingam, P.; Venkatakrishnan, K.; Tan, B. An atomic-defect enhanced Raman scattering (DERS) quantum probe for molecular level detection—Breaking the SERS barrier. *Appl. Mater. Today* **2019**, *16*, 28–41. [CrossRef]
13. Reguera, J.; Langer, J.; De Aberasturi, D.J.; Liz-Marzán, L.M. Anisotropic metal nanoparticles for surface enhanced Raman scattering. *Chem. Soc. Rev.* **2017**, *46*, 3866–3885. [CrossRef] [PubMed]
14. Bindhu, M.; Umadevi, M. Silver and gold nanoparticles for sensor and antibacterial applications. *Spectrochim. Acta Part A Mol. Biomol. Spectrosc.* **2014**, *128*, 37–45. [CrossRef] [PubMed]
15. Seney, C.S.; Gutzman, B.M.; Goddard, R.H. Correlation of Size and Surface-Enhanced Raman Scattering Activity of Optical and Spectroscopic Properties for Silver Nanoparticles. *J. Phys. Chem. C* **2008**, *113*, 74–80. [CrossRef]
16. Tiwari, V.S.; Oleg, T.; Darbha, G.K.; Hardy, W.; Singh, J.; Ray, P.C. Non-resonance SERS effects of silver colloids with different shapes. *Chem. Phys. Lett.* **2007**, *446*, 77–82. [CrossRef]
17. Oh, M.-K.; Shin, Y.-S.; Lee, C.-L.; De, R.; Kang, H.; Yu, N.E.; Kim, B.H.; Kim, J.H.; Yang, J.-K. Morphological and SERS Properties of Silver Nanorod Array Films Fabricated by Oblique Thermal Evaporation at Various Substrate Temperatures. *Nanoscale Res. Lett.* **2015**, *10*, 962. [CrossRef]
18. Rigó, I.; Veres, M.; Himics, L.; Tóth, S.; Czitrovszky, A.; Nagy, A.; Fürjes, P. Comparative Analysis of SERS Substrates of Different Morphology. *Procedia Eng.* **2016**, *168*, 371–374. [CrossRef]
19. Liu, K.-K.; Tadepalli, S.; Tian, L.; Singamaneni, S. Size-Dependent Surface Enhanced Raman Scattering Activity of Plasmonic Nanorattles. *Chem. Mater.* **2015**, *27*, 5261–5270. [CrossRef]
20. Garcia-Leis, A.; Garcia-Ramos, J.; Sanchez-Cortes, S. Silver Nanostars with High SERS Performance. *J. Phys. Chem. C* **2013**, *117*, 7791–7795. [CrossRef]
21. Liu, L.; Wu, Y.; Yin, N.; Zhang, H.; Ma, H. Silver nanocubes with high SERS performance. *J. Quant. Spectrosc. Radiat. Transf.* **2020**, *240*, 106682. [CrossRef]
22. Krajczewski, J.; Joubert, V.; Kudelski, A. Light-induced transformation of citrate-stabilized silver nanoparticles: Photochemical method of increase of SERS activity of silver colloids. *Colloids Surfaces A: Physicochem. Eng. Asp.* **2014**, *456*, 41–48. [CrossRef]

23. Nehra, K.; Pandian, S.K.; Bharati, M.S.S.; Soma, V.R.; Kumar, P.S.; Bharathi, M.S.S. Enhanced catalytic and SERS performance of shape/size controlled anisotropic gold nanostructures. *New J. Chem.* **2019**, *43*, 3835–3847. [CrossRef]
24. Parnklang, T.; Lamlua, B.; Gatemala, H.; Thammacharoen, C.; Kuimalee, S.; Lohwongwatana, B.; Ekgasit, S. Shape transformation of silver nanospheres to silver nanoplates induced by redox reaction of hydrogen peroxide. *Mater. Chem. Phys.* **2015**, *153*, 127–134. [CrossRef]
25. Bastus, N.G.; Merkoçi, F.; Piella, J.; Puntes, V. Synthesis of Highly Monodisperse Citrate-Stabilized Silver Nanoparticles of up to 200 nm: Kinetic Control and Catalytic Properties. *Chem. Mater.* **2014**, *26*, 2836–2846. [CrossRef]
26. Sun, Y.; Xia, Y. Triangular Nanoplates of Silver: Synthesis, Characterization, and Use as Sacrificial Templates for Generating Triangular Nanorings of Gold. *Adv. Mater.* **2003**, *15*, 695–699. [CrossRef]
27. Lide, D.R.; Frederikse, H.P.R. *CRC Handbook of Chemistry and Physics*, 74th ed.; CRC Press: Boca Raton, FL, USA, 1993–1994.
28. Ceballos, M.; Arizmendi-Morquecho, A.; Sanchez-Dominguez, M.; López, I. Electrochemical growth of silver nanodendrites on aluminum and their application as surface-enhanced Raman spectroscopy (SERS) substrates. *Mater. Chem. Phys.* **2020**, *240*, 122225. [CrossRef]
29. Macia, N.; Bresolí-Obach, R.; Nonell, S.; Heyne, B. Hybrid Silver Nanocubes for Improved Plasmon-Enhanced Singlet Oxygen Production and Inactivation of Bacteria. *J. Am. Chem. Soc.* **2018**, *141*, 684–692. [CrossRef]